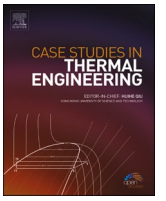
Case Studies in Thermal Engineering 55 (2024) 104191



Contents lists available at ScienceDirect

Case Studies in Thermal Engineering

journal homepage: www.elsevier.com/locate/csite



Numerical analysis of the heat transfer and pressure drop of a wavy fin and Kammtail tube condenser: An investigative study

Funda Erdem Şahnali [a,b,*], Ş. Özgür Atayılmaz [a], Zafer Gemici [a]

[a] Mechanical Engineering Department, Yıldız Technical University, Istanbul, 34349, Turkey
[b] Arçelik Research and Development Center, Istanbul, 34950, Turkey

ARTICLE INFO

Handling Editor: Huihe Qiu

Keywords:
Fin and tube heat exchanger
Tube shapes
Computational fluid dynamics
Experimental validation
Fin optimization

ABSTRACT

The aim of this study was to numerically investigate the factors affecting the air-side performance of an innovative condenser for a domestic refrigerator. Novel condenser with a smooth Kammtail tube form was investigated due to delaying flow separation. For the first time in the literature, the kammtail form was used instead of round or ellipse geometry in a finned tube heat exchanger, and the advantages of this form was demonstrated both experimentally and numerically. This study incorporated design parameters such as air velocity (0.5, 0.7, 1 m/s), number of tube rows (4 or 5), tube arrangement (inline, staggered), fin pitches (5, 7, 10, 5–7, 5–10, 7–10 mm), and fin arrangement (homogeneous or hybrid). The findings indicated that, for identical fin types and fin surface areas, the proposed Kammtail shape of 3 × 6 mm exhibited 19% lower pressure drop and 9% higher heat-transfer coefficient compared to the original circular tube profile. Furthermore, decreasing the fin pitches resulted in a 32.9–97% increase in static pressure drop, while the heat-transfer coefficient decreased by about 4.7–11.7%. The examination of two new designs revealed a marked reduction of 7–20.4% in the static pressure drop, a decline in air flow rate of 30%, an increase in heat transfer of 5.6–12.2%, and a corresponding decrease in the volume of the condenser of 20%. The numerical results of this study are in good agreement with experimental results, with deviations of less than 10%.

Nomenclature

c_p	specific heat, [$Jkg^{-1}K^{-1}$]
D	diameter of tube, [m]
D_h	Hydraulic diameter, [mm]
H	total width, [mm]
h	heat-transfer coefficient, [$Wm^{-2}K^{-1}$]
h_{out}	outlet heat-transfer coefficient, [$Wm^{-2}K^{-1}$]
k	thermal conductivity, [$Wm^{-1}K^{-1}$]
T_i	inlet temperature, [K]
T_o	outlet temperature, [K]
L	total length, [mm]

* Corresponding author. Mechanical Engineering Department, Yıldız Technical University, Istanbul, 34349, Turkey
E-mail address: funda.erdem@arcelik.com (F. Erdem Şahnali).

https://doi.org/10.1016/j.csite.2024.104191
Received 27 November 2023; Received in revised form 21 February 2024; Accepted 27 February 2024
Available online 1 March 2024
2214-157X/© 2024 The Authors. Published by Elsevier Ltd. This is an open access article under the CC BY-NC-ND license (http://creativecommons.org/licenses/by-nc-nd/4.0/).

A_{fin}	total area of the fins, [m^2]
A_{tot}	total area, [m^2]
$\dot{m}$	mass flow rate, [kg s^{-1}]
y^+	boundary layer thickness, [−]
F_p	fin pitches, [mm]
ΔT_{lm}	logarithmic temperature difference, [−]
RNG	Renormalization group
RANS	Reynolds-averaged Navier–Stokes
COP	coefficient of performance

Greek Symbols

ρ	Density, [kgm^{-3}]
μ	Dynamics viscosity, [Pa. s]
ϑ	kinematic viscosity, [m^2s^{-1}]
η^*	efficiency of the extended surfaces
ν	velocity, [$msec^{-1}$]

Subscripts

i, o	inlet and outlet of the condenser
ref	refrigerator
in	inlet
out	outlet
out,avg	average of outlet
f	fin
w	wall
tot	total
P	pressure drop, [Pa]
Q	heat-transfer rate, [W]
Re	Reynolds number, [−]
S_l	horizontal distance, [mm]
S_t	vertical distance, [mm]
h_{in}	inlet heat-transfer coefficient, [$Wm^{-2}K^{-1}$]
T	temperature, [K]
T_w	tube wall temperature, [K]
F	constant, [−]
u	freestream velocity, [ms^{-1}]
D_{fin}	diameter of the fin, [m]
h_{fin}	heat-transfer coefficient of fin, [$Wm^{-2}K^{-1}$]
Nu	Nusselt number, [−]
q	heat flux, [Wm^{-2}]
R_T	tube row number, [−]
H_l	height of condenser, [mm]
SST	Shear stress transport
CFD	computational fluid dynamics

1. Introduction

In accordance with a recent report published by the International Energy Agency [1], it has been established that domestic appliances are accountable for approximately 15% of the total global electrical energy consumption. Consequently, there is an imperative need to optimize the efficiency of household refrigeration systems with the objective of reducing their energy consumption. The efficiency of a refrigerator is contingent upon the performance of its cooling components, which predominantly employ a vapor-compression cycle to achieve cooling. Within this cooling system, condensers, acting as significant components, play a seminal role in determining the overall performance of refrigerators. Improving their performance is therefore crucial to reducing the rate of depletion of the planet's resources.

Various types of condenser configurations find applications in refrigeration systems, and their thermal performance is significantly influenced by the design characteristics of fins and tubes. One example of related research is the experimental study conducted by Wongwises et al. [2] to investigate the performance of a herringbone finned heat exchanger, analyzing the effects of varying fin thicknesses, fin spacings, and pipe row numbers. Their findings indicated that, for Reynolds numbers (Re_{D_c}) exceeding 2500, an increase in fin spacing led to a rise in the drag factor. Nuntaphan et al. [3] focused on the influence of tube diameter, fin spacing,

cross-tube spacing, and tube arrangement on the heat exchanger performance of spiral fins. Their study revealed that augmenting the tube diameter and fin height substantially elevated the pressure drop within the inline array configuration. Furthermore, Erek et al. [4] conducted numerical investigations with a specific emphasis on fin geometry to evaluate its effects on heat-transfer rates and pressure drops of finned-tube heat exchangers. Their study revealed a noteworthy influence of fin spacing on pressure drop. Kumar et al. [5] conducted a comprehensive examination of the thermal and hydraulic characteristics of plate and circular fins with varied geometrical parameters such as outer tube diameter, number of tube rows, tube spacing, fin pitch, and fin height. Their findings demonstrated that under conditions of constant Reynolds numbers, circular fins exhibited a heat transfer per unit pumping power that was 140–170% greater compared to plate fins. In another investigation conducted by Liu et al. [6], the utilization of perforated fins was found to enhance the heat-transfer efficiency of finned-tube heat exchangers characterized by wide fin spacing. Their results indicated a 6.3% reduction in heat-transfer rate at a Reynolds number of 750 when employing a fin pitch of 7.5 mm. Li et al. [7] devised an experimental methodology to investigate the influence of tube arrays and H-type fins on heat transfer and pressure drop. They examined various geometric parameters, including fin height, fin spacing, fin width, and tube pitches, particularly for high Reynolds numbers. Furthermore, they established correlations for the Euler and Nusselt numbers specifically for the air side of the heat exchanger configuration. The aim of the study conducted by Romero-Méndez et al. [8] was to investigate the impact of fin spacing on heat transfer in plate fin and tube heat exchangers and they provided valuable insights and recommendations for optimizing heat exchanger design and performance. They concluded that for small fin gaps, the flow was symmetric and of the Hele-Shaw type. As the gap increased, a separation region formed behind the cylinder. In a study by Wais et al. [9], numerical analyses were conducted to assess the performance of a finned-tube heat exchanger with eight different fin angles. Their findings indicated that the angle of louver inclination affects the flow direction, as well as heat transfer and temperature changes. Heat transfer was found to be 20.5% higher at a 45° louver angle compared to the current state. In another computational fluid dynamics (CFD) modeling investigation by Morales et al. [10], it was stated that specific geometric parameters and fin types contributed to the enhancement of the performances of fin-tube geometries. They determined that geometries featuring a greater surface-area-to-volume ratio were most effective in enhancing performance. Zhao et al. [11] systematically examined the influence of various parameters including row number, tube-to-tube distance, fin spacing, fin thickness, and Reynolds number on the thermal-hydraulic characteristics of rectangular fins employed in circular and elliptical tube heat exchangers. Their findings demonstrated that increasing the longitudinal tube slope, fin height, and fin width or reducing the cross-tube slope and axial fin pitch resulted in enhanced heat-transfer capabilities alongside increased air-flow resistance within the rectangular fin heat exchanger. To evaluate the thermal hydraulic performance of finned-tube heat exchangers with circular, oval, and flat tubes in inline and staggered arrays, the three performance evaluation criteria of area benefit factor, heat-transfer rate per unit fan power consumption, and heat-transfer rate per unit total power consumption were taken into account by Zeeshan et al. [12]. Pressure drop was reduced by 39.9% at a higher Reynolds number for the oval tube compared to the circular tube shape with an inline arrangement. Park et al. [13] performed a numerical analysis to assess the thermal performance of various combinations of louver and slit-fin configurations in comparison to slit fins. Their findings showed that an X-shaped slit-fin model with a fin pitch of 1.5 mm could serve as a viable alternative to a V-shaped corrugated fin with a 1.7-mm fin pitch, achieving substantial weight reduction of 11.7%. A numerical study was undertaken by Gholami [14] to investigate the thermal performance characteristics of a compact heat exchanger design with a novel fin design. In comparison to the base case, the design featuring a single corrugated fin with oval tubes and the three-corrugated-fin design demonstrated improvements in performance ranging from 5% to 15%. This improvement was attributed to the reduction of the dead zone behind the tube and pressure losses, resulting in improved flow mixing and an increase in the effective surface area. In another study, Lu et al. [15] investigated the effects of geometric parameters (fin spacing, tube spacing, fin thickness, and tube diameter) on the performance ($Q/\Delta P$ and COP) of a two-row finned-tube heat exchanger. They found that as the horizontal tube spacing increased, both $Q/\Delta P$ and COP increased. However, those values decreased with an increase in tube diameter and fin thickness. Pongsoi et al. [16] performed experimental investigations aimed at forecasting the consequences of varying fin spacings on the air-side performance of an L-foot spiral fin-tube heat exchanger within the Reynolds number range of 4000–15,000. Their findings indicated that both the air-side heat-transfer coefficient and the Colburn factor remained unaffected by alterations in the fin pitch. A study involving a numerical investigation of the impact of placing grooves on a half-ring-shaped fin to improve the flow patterns in a circular tube heat exchanger and its effects on heat transfer and flow structure was conducted by Lin et al. [17]. The use of grooved fins resulted in a reduction of the weak region formed behind the tube. At low Reynolds numbers and the same pumping power, grooved fins had a relatively weak effect. However, at high Reynolds numbers, the friction factor increased by 35%, the average Nusselt number increased by 10–40%, and thermal performance improved by 7–27% when compared to plain fins. The aim of the study by Gönül et al. [18] was to investigate wire-on-tube condensers with both experimental and numerical analyses, considering factors like wire diameter, tube diameter, wire pitch, and tube pitch at various air velocities. Their results showed that increasing the wire diameter reduced the heat transfer on the wire while increasing it on the tube. Widening the wire spacing reduced the average convection coefficients on both tubes and wires by approximately 7–8%. The effects of using helix wire finned tubes to enhance heat exchanger performance, reduce weight, and lower manufacturing costs were studied experimentally by Maghsoudali et al. [19]. They observed that helix wire fins outperformed spiral and serrated fins by 65% and 57%, respectively, in terms of thermal performance. Espindola et al. [20] developed a correlation for air-side heat-transfer coefficient prediction of natural draft wire-on-tube condensers in household refrigeration considering various geometric designs. They concluded that condenser height and wire/tube pitches were crucial for heat transfer. Additionally, optimizing the condenser design involved reducing wire and tube mass while maintaining heat duty. In another study, Arsana et al. [21] explored the role of geometric design in the performance of wire and tube heat exchangers, focusing on inline, single-staggered, and woven matrix wire and tube heat exchangers. They applied a combined experimental and numerical approach to optimize the wire and tube heat exchangers, considering parameters like wire diameter, tube spacing, and tube diameter. As a result, considering overall thermal performance, material mass, and manufacturing cost, the single-staggered wire and

tube heat exchanger was highlighted as the most efficient model among the three wire-tube configurations studied. In another previous study, Peker and Özkan [22] carried out an experimental investigation on a specific condenser type known as a hot-wall condenser with the aim of enhancing the overall performance of the refrigeration cooling cycle. That study's findings revealed the significant impact of variations in tube section form (O/D) on the rate of heat transfer in the condenser.

Due to delayed flow separation and a reduction in recirculation area, it is well known that the shape and size of the tube have a dominant effect on the convection coefficient and pressure drop. Thus, a "Kammtail form" - a smooth and streamlined geometry was proposed in this work. The novelty of this study lies in implementing a new Kammtail tube form equipped with a wavy fin, as opposed to the conventional wire-on-circular tube condenser, relying on various design parameters such as fin spacing, tube rows, tube arrangement, fin layout, and air velocity. Enhancing the wire-on-tube condenser's air side heat transfer efficiency is the primary goal, especially for low Reynolds number applications. To the best of the authors' knowledge, a finned tube heat exchanger using a kammtail tube form with a non-homogeneous wavy fin arrangement rather than circular or elliptical geometry was used for the first time in the literature.

2. Methodology

This study analyzed various tube and fin design features in a refrigerator coil condenser, as illustrated in Fig. 1, by employing numerical models and experimental methods. To increase the efficiency of the conventional wire-on-tube condenser, we used a modified Kammtail tube design along with a wavy fin as an alternative technique. After verifying the process, we conducted optimization analyses to identify the optimal configuration in comparison to the original condenser. In order to attain a thorough understanding of how tube and fin characteristics impact air-side heat transfer and pressure drop, a condenser model was established utilizing analysis and experimentation undertaken within the air duct. The secondary effects on the bottom of the refrigerator cabinet were deliberately disregarded in order to decrease the computational burden and facilitate a wider range of optimization assessments. This approach not only boosted computational efficiency but also reduced potential errors associated with modeling the complete geometry.

Throughout the study, a fixed temperature of 45 °C was maintained on the tube's surface, with temperature variations being negligible. Temperature measurements were carried out with great care along the entire length of the tube during the experimental trials to maintain this constant value. Precise temperature control was achieved using an expansion valve and optimal flow, resulting in temperature variation of approximately 1 °C throughout the length of the tube. The accurate temperature control facilitated the assumption of a uniform surface temperature, negating the necessity of computing the internal convection coefficient during the computational analysis. It is worth noting that the air-side heat-transfer coefficient of the heat exchangers is a crucial factor affecting a fridge's cooling efficiency. The aim of this investigation was to increase the air-side heat-transfer coefficient of the condenser utilized for heat dissipation in the system. The results confirmed a significant improvement in the heat-transfer coefficient, which ultimately led to enhanced system efficiency.

The wire-on-tube cross-flow coil condenser utilized in this research is displayed in Fig. 1. The condenser consists of circular tubes arranged in a grid formation, with 9 vertical rows and 5 horizontal rows, and wire-type fins placed on the air side. The tubes are aligned in line with tube length of 135 mm and diameter of 4.8 mm. Both the fin and the tube comprise stainless steel materials.

2.1. Numerical simulation

This study analyzed the heat transfer and fluid flow characteristics on the air side of the condenser with a focus on forced convection conditions. For this analysis, we used ANSYS 2022 R^2 FLUENT® software, which is a finite volume solver used to solve Navier-Stokes and turbulence models equations. In this computational framework, we considered the air to be an incompressible ideal gas and assumed that its flow was in a steady state.

2.1.1. Geometrical modeling

The geometry of the entire condenser was simulated in a 3D model to explore the impact of tube and fin characteristics and parameters on both heat transfer and pressure drop. A unique Kammtail tube design was employed, which included wavy fins. For ease of modeling, improved mesh quality, and reduced computational time, the condenser was simulated separately, within an air duct, independently of the refrigerator body. Fig. 2 presents the wire-on-tube condenser arrangement. To ensure uniform inlet velocity and

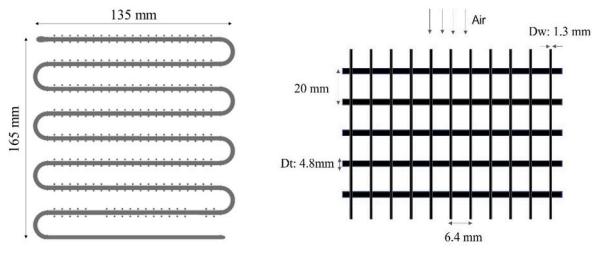


Fig. 1. Representation of wire-on-tube condenser.

prevent recirculation in the flow, the computational domain was expanded by a distance of 10*D* at the inlet and 20*D* at the outlet, where *D* denotes the tube diameter [23]. The dimensions L, *H*, and *S* had specific values of 140 mm, 190 mm, and 20 mm, respectively.

2.1.2. Discretization

To improve the quality of the mesh and decrease the number of elements, a type of poly-hex mesh element was utilized. The mesh characteristics can be found in Table 1, while Fig. 3 displays the mesh. A boundary layer region incorporating a smooth transition of four layers was established around the tubes to precisely approximate the change in velocity and temperature gradient.

Mesh independence analysis was performed to identify the most suitable solution with minimal error and reduced computational time. Upon increasing the mesh number from 15 to 20 million elements, the maximum variation noted in the total heat-transfer rate across the flow amounted to 3.4%, as illustrated in Fig. 4. Therefore, all analyses were executed with 20 million mesh elements to minimize the difference between CFD and experimental results. Using the poly-hex mesh element type depicted in Fig. 3, the optimal configuration resulted in approximately 20 million elements and a maximum quality of 0.75. This outcome was deemed acceptable, as the goal was to approach a value of 1 as closely as possible [24].

2.1.3. Governing equations

The Navier-Stokes equations denoted in Eqs. (1)–(3) indicate the conservation of mass, momentum, and energy, respectively [23,24]:

$$\frac{\partial u_i}{\partial x_i} = 0 \tag{1}$$

$$\rho u_j \frac{\partial u_i}{\partial x_j} = -\frac{\partial P}{\partial x_i} + \frac{\partial}{\partial x_j}\left((\mu + \mu_t)\frac{\partial u_i}{\partial x_j}\right) \tag{2}$$

$$\rho c_p \left(u_i \frac{\partial T}{\partial x_j}\right) = \frac{\partial}{\partial x_j}\left((k + k_t)\frac{\partial T}{\partial x_j}\right) \tag{3}$$

x_i and x_j represent the coordinates of the Cartesian system, namely the x, y, and z axes.

The SST k-ω turbulence model is widely preferred because of its enhanced reliability and accuracy in adverse pressure gradient flows. The model outlined in this research has the ability to be employed over a wide range of Reynolds numbers, including low and high values. Additionally, its suitability extends to areas situated close to the wall as well as those located at a considerable distance [25,26]. The consideration of turbulent viscosity requires the transportation of shear stress caused by turbulence. The transport equations for turbulent kinetic energy (k) and specific dissipation rate (ω) are employed in steady-state conditions and take the following form:

$$\frac{\partial}{\partial x_i}(\rho k u_i) = \frac{\partial}{\partial x_j}\left(\Gamma_k \frac{\partial k}{\partial x_j}\right) + G_k - Y_k + S_k + G_b \tag{4}$$

$$\frac{\partial}{\partial x_i}(\rho \omega u_i) = \frac{\partial}{\partial x_j}\left(\Gamma_\omega \frac{\partial \omega}{\partial x_j}\right) + G_\omega - Y_\omega + D_\omega + S_\omega + G_{\omega b} \tag{5}$$

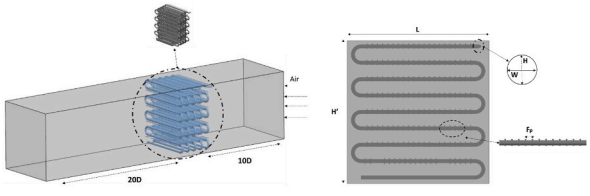
Here, G_k denotes the creation of turbulent kinetic energy, while G_ω represents ω generation, Γ_k and Γ_ω respectively refer to the effective diffusivity of k and ω, and Y_k and Y_ω represent the dissipation of k and ω. Additionally, D_ω is the cross-diffusion term, while S_k and S_ω denote source terms defined by the user. Finally, G_b and $G_{\omega b}$ account for buoyancy. Further exploration of these factors is possible based on previous work [24,27].

The ideal gas state equation is given in Eq. (6):

$$PV = \rho RT \tag{6}$$

2.1.4. Boundary conditions

The SST k-ω turbulence model was chosen for fluid flow analysis because it was recommended for low Reynolds number applications by Wais, Gönül et al., and Mangrulkar et al. [9,28,29]. Furthermore, a previous study [27] revealed that the SST model



(a) Perspective view of the geometry (b) Side view of the condenser

Fig. 2. Geometry used in the CFD modeling.

Table 1
Mesh settings used in ANSYS FLUENT software.

Parameters	Values
Defaults and sizing	
Minimum size	0.25 mm
Growth rate	1.2
Maximum size	16 mm
Size function	Curvature & proximity
Curvature normal angle	18
Face sizing (tube and fin)	1 mm
Inflation	
Boundary	Tube
Inflation option	Smooth transition
Number of layers	4
Transition ratio	0.272
Growth rate	1.2

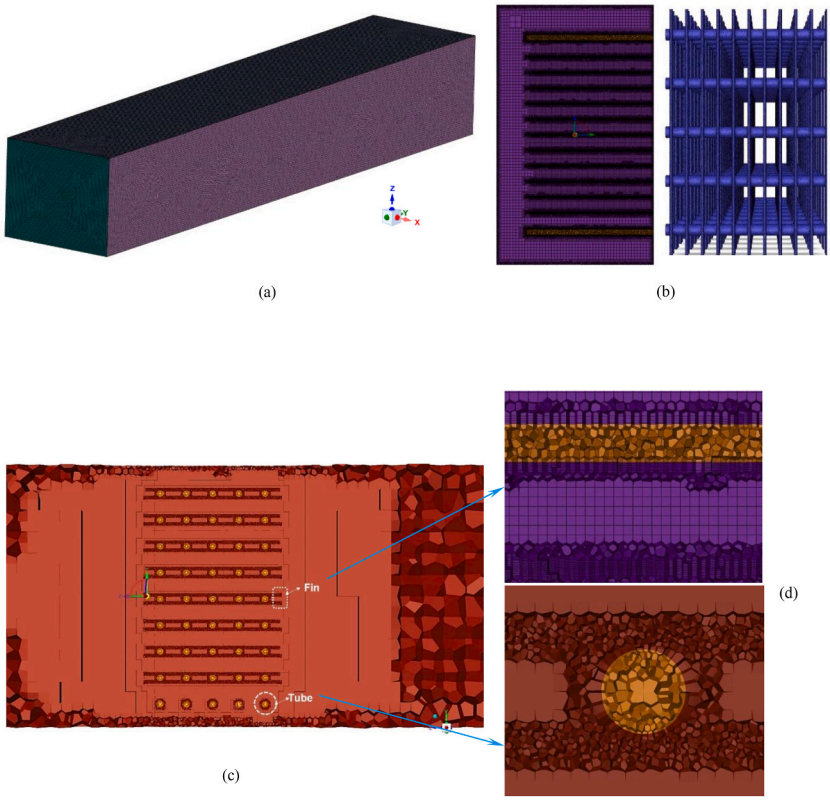


Fig. 3. Mesh structure: (a) general view of the meshed volume, (b) condenser detail, (c) fluid and solid domain detail, (d) tube and fin surface detail.

produced results indistinguishable from those of data with y^+ values in the range of 0.1–100. A refined boundary layer mesh was utilized in this study, with maximum y^+ values of 1.7 for the fin region and 5 for the tube region.

The model's boundary conditions are explained in Table 2 and depicted in Fig. 5. Inlet air velocity remains constant at 1 m/s, with the side walls considered adiabatic, meaning that no heat transfer occurs between them and the surroundings. The condenser's surface temperature is taken to be 45 °C, with incoming air temperature of roughly 25 °C obtained through experiments. At the outlet, the boundary condition is specified as 0 Pa pressure. For easier modeling, we presumed symmetry boundary conditions. The condenser was constructed using steel.

Table 3 presents an all-encompassing overview of the solver parameters and discretization methods utilized in this study. Convergence thresholds of 10^{-6} for continuity and 10^{-9} for energy were established.

2.2. Experimental setup and validation

To confirm the validity of the numerical model in terms of total heat-transfer rate and pressure drop, thermal and hydraulic experiments were carried out on the wire on the tube condenser using appropriate experimental setups as described below. We also detail

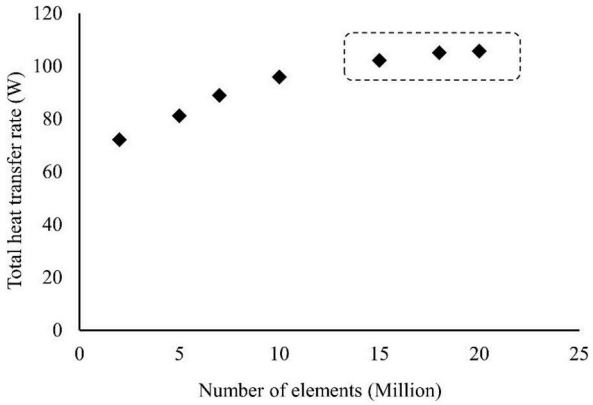


Fig. 4. Mesh independence analysis.

Table 2
List of boundary conditions.

The incompressible ideal gas and turbulence flow	Incompressible flow assumption is applicable for the pressure ranges and velocities under consideration with negligible errors [30]. Reynolds is higher than 4000, so the flow is turbulent.
Constant physical properties for fluid and materials	Under the investigated temperature ranges, thermophysical properties are almost constant [30].
No mass transfer is being taken place	There is no mass transfer for the considered problem.
Perfect contact assumption between fin and tube	There is fully welded joints.
Thermal radiation are negligible	Forced convection exists and its order is quite high, so it is possible to neglect radiation with respect to forced convection.
Smooth surface conditions for the fin-and-tube	Under turbulence flow, roughness effects can be neglected [24].
The flow and heat transfer are in steady state	It is investigated under steady conditions.
Adiabatic boundary condition for side walls	Heat transfer from the side walls can be neglected with respect to the heat transfer from the tubes to the air.
At the inlet: $u = u_{in}$ and $T = T_{in}$	These are adjusted test conditions
At the outlet: 0 Pa pressure	The outlet is open to the atmosphere
Constant temperature for the fin-and-tube walls	There is phase change inside the tube almost at constant temperature.
Symmetry boundary conditions assumption	The geometry has symmetry.

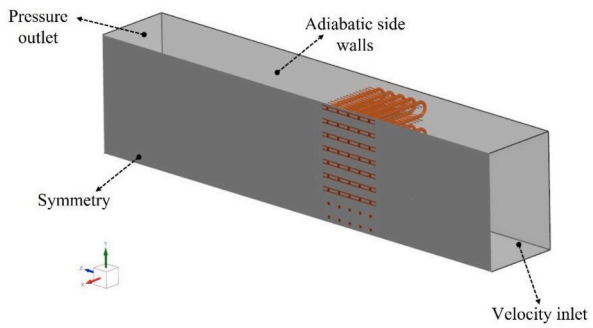


Fig. 5. Boundary conditions in the CFD model.

the methodology employed to acquire the outcomes.

2.2.1. Experimental setup for determining pressure drop

A wind tunnel was constructed in accordance with the AMCA 210-85 standard [31] for the purpose of obtaining the pressure-volume flow-rate curve. Table 4 presents comprehensive details regarding the wind tunnel and data acquisition equipment employed in the study.

The wind tunnel is 1.76 m in length, 0.84 m in width, and 0.84 m in depth. The second section of the tunnel holds three nozzles,

Table 3
Solver settings and discretization methods.

Pressure-velocity relation	Coupled
Gradient discretization	Least squares cell-based
Pressure discretization	Second-order
Momentum discretization	Second-order upwind
Turbulent kinetic energy discretization	Second-order upwind
Specific dissipation rate discretization	Second-order upwind
Initialization	Hybrid initialization

Table 4
Specifications of measuring instruments.

Instrument	Brand	Model/range	Feature/sensitivity
Datalogger	Agilent	34,970 A	–
Computer	HP	–	–
Exhaust fan	EBM	–	230 V/1.75 A
Differential pressure manometer	Furness	FCO510	±0.01%
T-type thermocouple	Omega Engineering	−100 to 370 °C	±0.3 °C
Nozzle	Woods of Air Movement	–	4 ± 0.005 cm^2

measuring 0.88, 1.6, and 3 inches, respectively. During the measurements, the selection of the specific nozzle to be opened or closed was decided through reference to established characteristic curves for flow rate and pressure. The screens were positioned consecutively in different sections of the tunnel to guarantee consistent airflow, thereby reducing measurement errors resulting from turbulence.

The experimental duct's airflow was directed towards the condenser, positioned at the center of the duct made of plexiglass material, from left to right. An exhaust fan facilitated this air flow, as depicted in Fig. 6. It was then directed into the wind tunnel and subsequently discharged to the wind tunnel's outlet. The pressure drop on the air-side of the condenser was measured at different levels of airflow velocities and was later compared to the CFD outcomes.

2.2.2. Experimental setup for determining thermal performance

The experimental setup was designed according to IEC 62552:2015 standard [32], which is a standard guideline of the International Electrotechnical Commission (IEC) for household refrigerators. Table 5 outlines the ranges and sensitivities of the equipment used in the experimental setup, as also illustrated in Fig. 7. The test room's temperature was kept constant throughout the experiment using an exhaust heater and an air conditioning system.

The experimental apparatus used to test the wire-on-tube condenser illustrated in Fig. 7 comprised numerous components including a test bench, valves, a compressor, a datalogger, a water conditioning unit, a computer, a flowmeter, and an air conditioning system. To record temperatures as required, multiple T-type thermocouples and two resistance temperature detectors (RTDs) were employed. Varying air inlet velocities (0.7, 1.0, and 1.2 m/s) were applied during the experiments, with three repetitions carried out. The data were collected assuming that the system operated continuously to validate the experiment. Each experiment lasted at least 60 min and commenced when the system approached steady-state conditions. Temperature measurements were taken at 1-sec intervals and then averaged for each recorded parameter in every experiment.

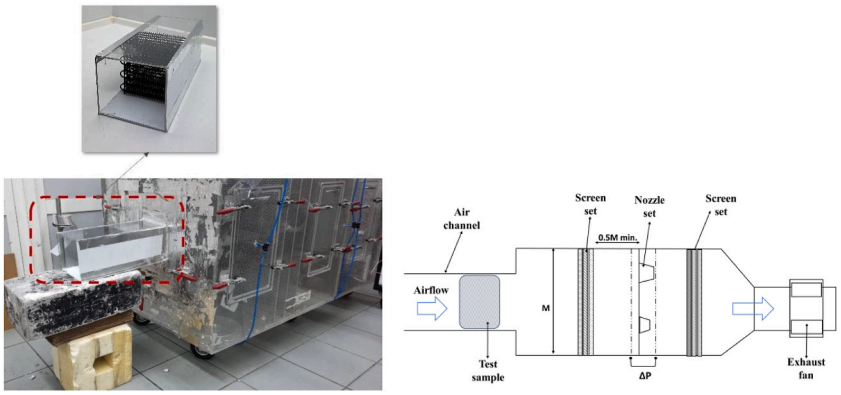


Fig. 6. (a) Experimental setup of wind tunnel, (b) schematic diagram of test apparatus.

Table 5
List of equipment used in the experimental setup.

Instrument	Brand/model	Range	Feature/sensitivity
Datalogger	Agilent 34,970 A	–	–
Computer	HP	–	–
Water conditioning unit	Labo	20 L/−25 to 100 °C	±0.1 °C
Flowmeter	Endress + Hauser	Max. 450 kg/h	±0.25%
Thermometer	Testo 174H	−20 to 70 °C	±0.5 °C
Air conditioner	LG	12,000 BTU	–
Ex-Proof heater	Scottcan	Max. 180 °C	2300 W/240 V
RTD	Fluke	−100 to 100 °C	±0.025 °C
T-type thermocouple	Omega Engineering	−100 to 370 °C	±0.3 °C

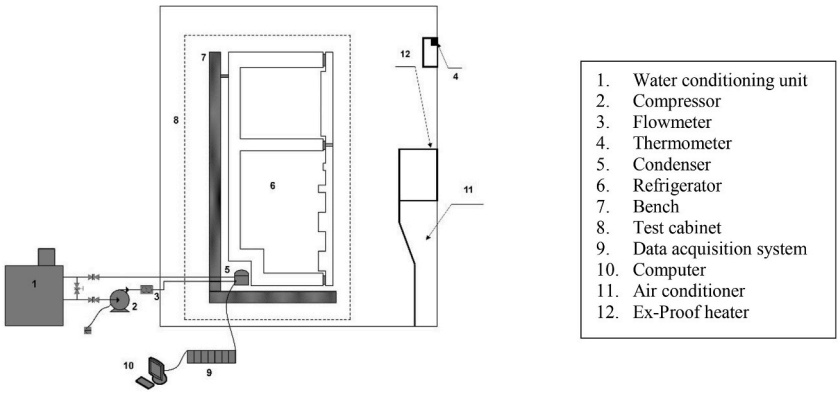


Fig. 7. Arrangement for testing condenser performance [32].

Fig. 8 displays the experimental setup located inside a temperature-regulated chamber. The wire-on-tube condenser was situated beneath the cabinet base, as depicted in the figure. The refrigerant, R600a, was utilized in a quantity of 50 g, and the temperature of the condenser's surface was 45 °C. A water conditioning unit and an electronic expansion valve were employed to establish thermal stability at an evaporation temperature of −10 °C. Throughout the tests, the temperature in the room was consistently maintained at 25 °C while the average air velocity was set at 1 m/s. The pressure and temperature sensors demonstrated accuracy of ±0.5% and ±0.3 °C, respectively.

2.2.3. Data evaluation

The experimental setup included temperature and pressure sensors placed at the air-side inlet and outlet of the condenser. Additionally, a flowmeter was used to determine the mass flow rate of the refrigerant circulating within the conditioning unit. The collected data were utilized to calculate the overall heat transfer ($Q_{outside}$); this represents the amount of heat that was extracted from the condenser. The temperature of the condenser's surface was 45 °C. The experiments were conducted under ambient conditions at a temperature of 25 °C. The results were evaluated focusing solely on convective heat transfer.

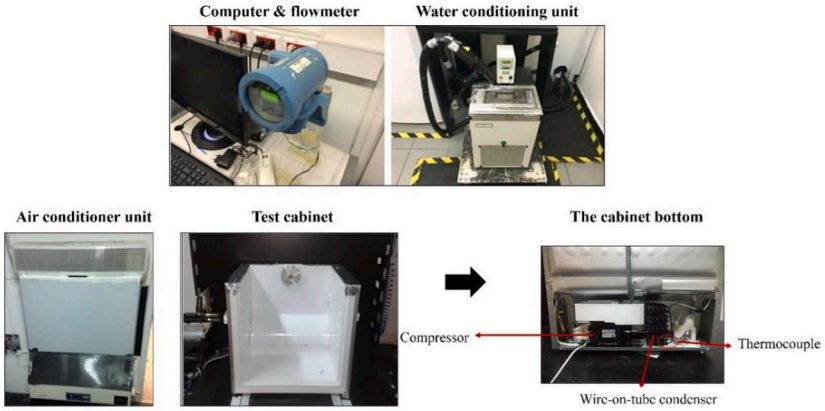


Fig. 8. Experimental setup in climate chamber.

Heat dissipation from the refrigerant in the condenser tube takes place through three mechanisms: convection inside the tube, conduction through the thickness of the tube, and convection outside the tube (radiation is neglected). The mathematical representation of heat loss/dissipation from the refrigerant through the condenser is as follows:

$$\dot{Q}_{ref} = \dot{m}\Delta h = \dot{m}(h_{out} - h_{in}) \tag{7}$$

Here, $\dot{m}$ and Δh refer to the mass flow rate and enthalpy difference of the refrigerant, respectively.

Since the surface temperature of the condenser was determined to be about 45 °C, heat transfer could be calculated without utilizing the convection coefficient of the inner surface and the thermal conductivity of the tube. Only the air-side heat-transfer coefficient was necessary. Accordingly, the heat transfer to the air on the air side of the condenser was calculated as follows:

$$\dot{Q}_{outside} = h\eta^* A_{tot} F \Delta T_{lm} \tag{8}$$

The overall surface area equals the total fin area and the total tube area combined, where $A_{tube} = \pi D_{tube} S_{tube}$, $A_{fin} = \pi D_{fin} S_{fin} N_{fin}$.

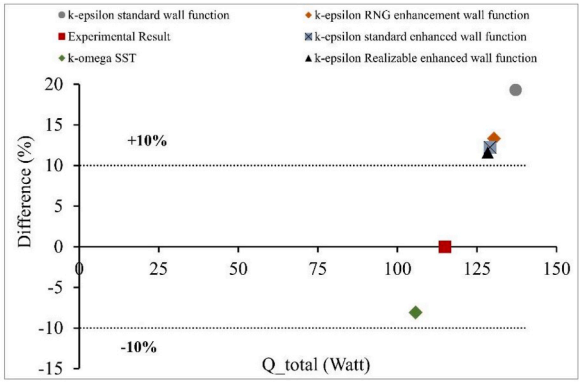
Here, the heat-transfer coefficient, fin efficiency, total outside heat-transfer area, correction factor, and mean logarithmic temperature difference between the air and refrigerant are denoted by h, η^*, A_{tot}, F, and ΔT_{lm}, respectively. F is equal to 1 in this instance as the surface temperature of the condenser is constant. The mean logarithmic temperature difference can be calculated using Eq (9):

$$\Delta T_{lm} = ((T_i - T_w) - (T_o - T_w)) \Big/ \left(\ln\left(\frac{T_i - T_w}{T_o - T_w}\right)\right) \tag{9}$$

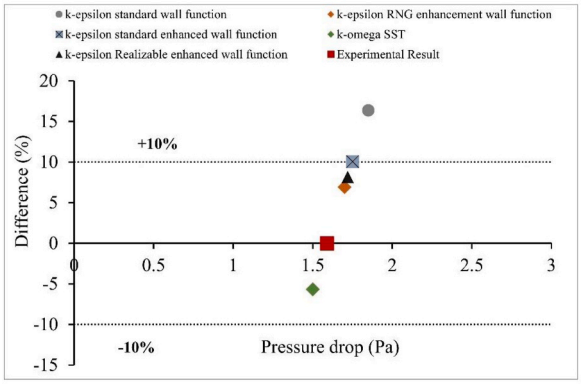
Here, T_w is the constant surface temperature of the condenser, and T_i and T_o represent the average air temperatures of the inlet and outlet of the condenser, respectively.

The change in temperature along the length of the wire, between the tubes, is reflected by fin efficiency. The performance of wire-on-tube condensers is significantly influenced by the efficiency of the fins, which is a critical factor. The equations put forward by Lee et al. [33] were employed to evaluate fin efficiency while considering the adiabatic fin tip boundary condition:

$$\eta^* = 1 - \left(A_{fin} / A_{tot}\right)\left(1 - \eta_f\right) \tag{10}$$



(a)



(b)

Fig. 9. Comparison of heat-transfer rates (a) and pressure drop (b) as calculated by CFD method for different turbulence models with experimental result (at 1 m/s air velocity).

$$\eta_f = \tanh[mL]/mL \tag{11}$$

$$m^2 = 4h_{fin} \,/\, \left(k_{fin} D_{fin}\right) \tag{12}$$

Here, A_{fin} denotes the total surface area of the fins, h_{fin} is the heat-transfer coefficient linked to the fins, D_{fin} specifies the diameter of the fins, k represents the thermal conductivity of the fins, and η_f signifies the efficiency of the extended surfaces that experience no heat transfer from the fin tip. m represents the temperature gradient on wires, while L represents half of the S_{tube} value.

The air-side Reynolds numbers and heat-transfer coefficients can be calculated as follows:

$$Re_D = \rho v D/\mu \tag{13}$$

$$h = \dot{Q}_{outside}/A\Delta T_{lm} \tag{14}$$

The Nusselt numbers can be computed by taking the tube diameter as the characteristic length, as shown in Eq. (15):

$$Nu_D = \frac{hD}{k} \tag{15}$$

The total heat gained by the air ($\dot{Q}_{tot}$) is equivalent to the heat loss of the refrigerant ($\dot{Q}_{ref}$) as well as the heat transfer occurring through the thickness of the tube and fins ($\dot{Q}_{outside}$). Eq. (16) is applied to compute the total heat:

$$\dot{Q}_{tot} = \dot{m} c_p (T_o - T_i) \tag{16}$$

2.2.4. Validation of the numerical model

Several studies in the literature have employed turbulence models to investigate flow disturbances at low Reynolds numbers under similar conditions [6,11,18,33]. In this study, analyses were conducted to examine the impact of different turbulence models, namely the k-ε standard wall, k-ε RNG, k-ε realizable, and k-ω SST models, on the obtained solution results. The primary objective was to identify the turbulence model that exhibited the closest agreement with the experimental data.

As a result of experimental trials, the total heat transfer and static pressure drop for air velocity of 1 m/s were calculated to be approximately 115 W and 1.59 Pa, respectively. Based on the findings presented in Fig. 9, it was concluded that the best results for the experimental research were obtained using the k-ω SST model, which demonstrated differences of less than 10%. Subsequent parametric tests were conducted based on this specific model.

Table 6 displays the results of the CFD analysis of pressure drop and heat-transfer rate at an air velocity of 1.0 m/s. Fig. 10 presents the accompanying velocity and pressure contours. These results were compared to the relevant experimental data. Based on the CFD results, the condenser dissipated 105.7 W of heat, causing a pressure drop of 1.5 Pa. To verify the numerical model's validity, we ensured that the uncertainty of the heat-transfer coefficient equivalent to the uncertainty of the heat-transfer rate, as explained in Section 2.2.5, did not deviate by more than 10%. The maximum uncertainty value of the heat transfer was determined to be 2.54%.

In order to ascertain the validity of the CFD study findings related to the air-side pressure drop, wind tunnel measurements were used to create the air velocity curve variations for the original condenser. The pressure drop for the original condenser was measured as 1.59 Pa with an average air inlet velocity of 1.0 m/s. The analysis of both the experimental and CFD data, as shown in Fig. 11, consistently indicated a margin of error of less than 10%.

2.2.5. Uncertainty analysis

A thorough examination of uncertainty was performed on the experimental parameters that were measured. The thermocouples were connected to a datalogger, specifically the Keysight 34970A–34901A multiplexer, and were calibrated using the Fluke 54 reference device, which has an accuracy of ±0.3 K. The complete temperature measurement system, consisting of the thermocouple, multiplexer, and data logger, has an accuracy of ±0.3 K. Table 7 displays the measured parameters and the accompanying equipment.

Eq. (17) was used to calculate the heat-transfer rate in watts:

$$\dot{Q}_{air} = \dot{m} c_p (T_{out} - T_{in}) \tag{17}$$

Here, $\dot{Q}_{air}$ is the heat-transfer rate (W), T is the temperature (K), and c_p is the specific heat (J/kg).

The equation suggested by Kline and McClintock [34] was employed to determine the uncertainty associated with the heat-transfer rate:

$$w_r = \sqrt{\left(\frac{\partial R}{\partial v_1} w_1\right)^2 + \left(\frac{\partial R}{\partial v_2} w_2\right)^2 + \ldots \left(\frac{\partial R}{\partial v_n} w_n\right)^2} \tag{18}$$

Table 6
CFD results of original finless condenser.

D_h (mm)	A_{total} (m^2)	A_{fin} (m^2)	Air velocity (m/sec)	$T_{out,avg}$ (K)	$Q_{outside}$ (W)	ΔP_{static} (Pa)	h (W/m^{2}K)	q (W/m^2)
4.8	0.22	0.13	1.0	300.6	105.7	1.5	25.8	480.5

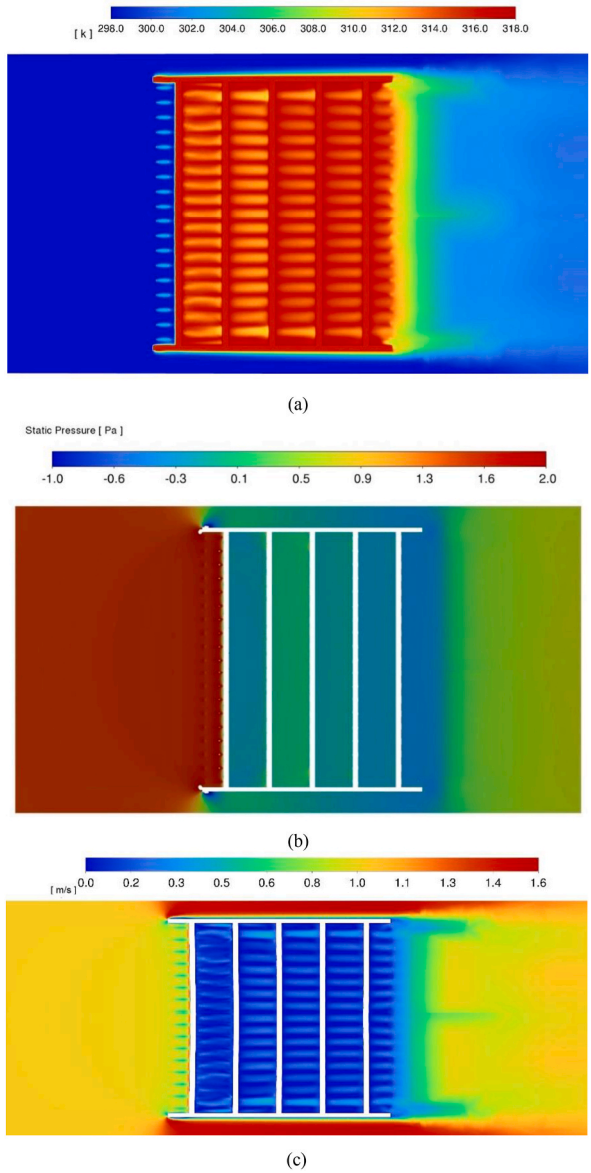


Fig. 10. (a) Temperature contour, (b) static pressure contour, and (c) velocity contour on symmetry plane (middle of the model) for the wire-on-tube condenser (air flow is from left to right).

Here, w represents the uncertainty in result R, which is a function of parameters v_1, $v_2 \ldots v_n$ and their respective uncertainties w_1, $w_2 \ldots w_n$. With these parameters taken into consideration, the uncertainty in the heat transfer can be amended as follows:

$$w_Q = \sqrt{\left(w_1 c_p (T_{out} - T_{in})\right) T_{out} - T_{in}\right) w_1 {c_p}^2 + \left(w_2 \dot{m} c_p\right)^2 + \left(w_3 \dot{m} c_p\right)^2} \tag{19}$$

Here, w_Q represents the uncertainty in the heat transfer, w_1 represents the uncertainty in the mass flow rate, and w_2 and w_3 represent the uncertainties in the corresponding temperatures.

Accordingly, the maximum uncertainty in the heat transfer was found to be 2.54% (Table 8). By employing Eq. (19) and the data from Table 6, the maximum uncertainty in the airflow velocity was determined to be 1.33%.

2.3. Geometric parameters

Aerodynamic forces arising from fluid-solid interactions are affected by the object's shape and fluid velocity, and by viscosity [35]. The impact of tube shape and aspect ratio on the aerodynamic performance and flow separation can be substantial. The presence of a circular shape generates notable drag resulting from pressure imbalances along the flow direction. Separation arises from an unfavorable pressure gradient encountered when the flow expands, thereby reducing the area of contact between the surface and the fluid,

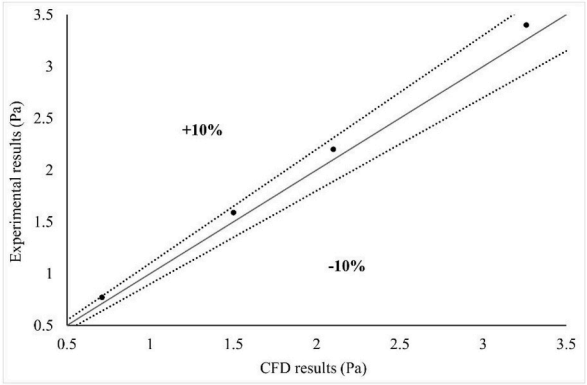


Fig. 11. CFD results with experimental data for static pressure drop.

Table 7
Accuracy values of measurements.

Sensor	Accuracy
Flowmeter	0.25%
Temperature	±0.3 K
Pressure	20 ± 0.15 Pa

Table 8
The uncertainty in the heat transfer.

	T_1 (C)	T_2 (C)	c_p (kj/kgC)	$\dot{m}$ (kg/sec)	Uncertainty (%)
Test-1	25.1	28.2	3.71	0.0101	2.40
Test-2	25	28.1	3.71	0.0098	2.54
Test-3	24.8	27.7	3.71	0.0105	2.35

and subsequently decreasing the rate of heat transfer. Therefore, this study was conducted using a novel design that presents a Kammtail tube shape and wavy fins characterized by a streamlined structure to delay flow separation. The aim was to enhance the aerodynamic efficiency of the existing condenser that has circular tubes and wire fins. To conduct a thorough comparison of air-side performance using numerical studies, we employed a profile with a Kammtail form of 3 × 6 mm (H × W), offering a smaller heat-transfer tube area than the original circular one (Fig. 12).

This study examines the impact of air velocity, fin pitches, row number of tubes, and layout of tubes and fins on pressure drop reduction and heat-transfer rate improvement. Table 9 displays the parameters investigated and their respective ranges.

As the temperature differential between the air and the refrigerant lessens, heat transfer decreases in the direction of flow. To increase condenser efficiency, the fins were positioned and studied in homogeneous and hybrid arrangements. Fig. 13 shows three fin pitches that were tested in both configurations. In the hybrid fin arrangement, the condenser's front half displays closely spaced fins while the rear has fins that are widely spaced, all in line with the flow direction.

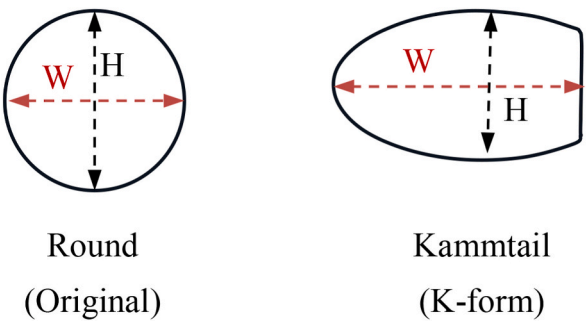


Fig. 12. Original and proposed tube shapes.

Table 9
Geometric parameters for CFD analysis.

Factor	Values
ν, Air velocity (m/sec)	1, 0.7, 0.5
F_p, Fin pitches (mm)	10, 7, 5, 5–7, 7–10, 5-10
R_T, Tube row number	5, 4
T_A, Arrangement of tubes	Inline, staggered
F_A, Fin arrangement	Homogeneous, hybrid

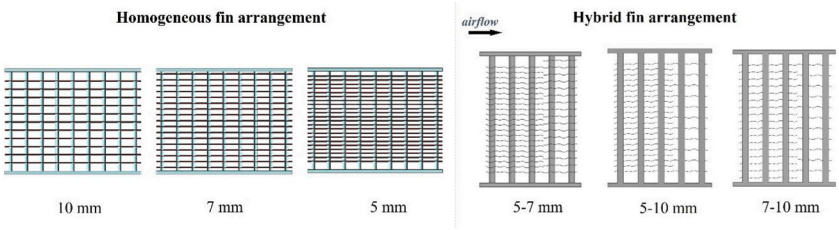


Fig. 13. Fin arrangement.

3. Results and discussion

After validating the numerical model through experimentation on the original condenser, air velocity, fin pitch, tube row number, and fin and tube arrangements were used as input parameters in a parametric study. These findings were then compared with the results for the original coil condenser. The "Original" point shown in the graphs below represents the numerical results for the original wire-on-tube condenser.

As illustrated in Fig. 14, the kammtail form configuration with dimensions of 3 × 6 mm exhibited a diminished low-velocity dead zone and a decreased recirculation area behind the tube in comparison to the original tube, attributable to the influence of surface shape. This explains the reduction in pressure drop for similar values of heat-transfer capacity when comparing Case-2 and Case-3 shown in Table 10. The locations denoted as "S," corresponding to the x-wall shear stress reaching 0, were identified at 0.59 and 0.78 for the circular and k-form 3 × 6 mm configurations, respectively. These results indicate that the alternative tube designs shifted the separation point and increased the contact area.

To assess the effect of the new Kammtail tube design on air-side performance, we introduced a wavy fin (Case-2) with spacing of 10 mm to the original circular tube profile. This was then compared to the Kammtail tube profile (Case-3) under the same conditions. In comparison to the original condenser design (Case-1), Case-2 had 16.3% growth in overall surface area, a 38% increase in pressure drop, and a 3% improvement in the overall heat-transfer coefficient. Compared to the Case-3 design, surface area, pressure drop, and heat-transfer coefficient were 12.3%, 19%, and 9% lower, respectively. Total heat transfer rate for the Case-3 design was found to be up to 22.8% higher than the original. For identical fin types and fin surface areas, the Kammtail tube configuration was found to have a superior heat transfer coefficient and lower pressure drop as opposed to the original circular tube shape (Table 10). This result showed the effect of tube shape on the pressure drop under the same fin type and fin surface area conditions.

Fig. 15 shows the variation of the static pressure drop in the inline tube arrangement of the Kammtail tube condenser for different air velocities and tube row numbers at different fin spacings. As expected, when the air velocity increases from 0.5 m/s to 1 m/s, the static pressure drop on the condenser increases by up to 66.6% for tube row numbers of 5 and 4. As the fin pitch decreases, the total surface area rises, resulting in an increase in friction. Consequently, there is an increase of 32.9%–97% in the static pressure drop depending on the velocity of the air. The reduction of tube rows from 5 to 4 led to a decrease in total surface area and flow resistance in the direction of flow. Consequently, the pressure drop decreased in the range of 12.1%–16.6%. When comparing the Kammtail tube condenser to the original condenser, it was found that at an air velocity of 0.7 m/s and a tube row number of 4, the pressure drop decreased by 5.1–40.9% depending on the fin spacing. This information is illustrated in Fig. 15.

As shown in Fig. 16, increasing air velocities led to an increase in the convection heat-transfer coefficient within a range of 18–33.4%. The heat-transfer coefficient was found to be up to 10% higher, particularly for the lower number of tube rows in the homogeneous fin arrangement, which was in line with expectations. As the surface area increases, the convection coefficient experiences a reduction of about 4.7–11.7% at all air velocities if the fin pitch decreases from 10 mm to 5 mm for a homogeneous fin arrangement, as displayed in Fig. 16. Compared to the homogeneous fin arrangement, the heat-transfer coefficient in the hybrid fin arrangement improved by about 10%.

As shown in Fig. 16, the convection heat-transfer coefficient of the Kammtail tube condenser decreased 7–13% depending on the fin spacing for tube row number of 4 and air velocity of 0.7 m/s due to the increase in total surface area up to 35.5% compared to the original condenser for 1 m/s air velocity and tube row number of 5. Furthermore, total heat transfer rate increased by 4.2%–23.8%.

Figs. 15 and 16 show that when the tube rows decrease from 5 mm to 4 mm for the new Kammtail tube design, pressure drop ranges from −58.7% to 110.7%, the convection heat transfer coefficient varies between −23% and 28.9% depending on the fin spacing. Additionally, it resulted in a change in the heat transfer value between −21.6% and 62%.

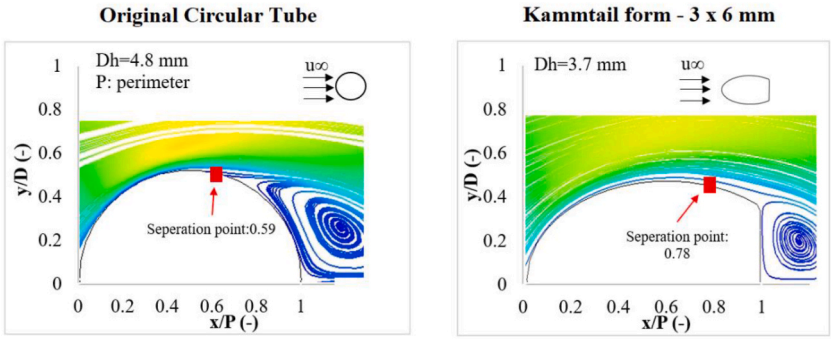


Fig. 14. Separation points and velocity streamline profiles.

Table 10
Tube effect results compared to the original condenser.

	Case-1	Case-2	Case-3
	Original wire-on-tube condenser	Original tube with wavy fin	Kammtail tube with wavy fin
Tube profile	Circular	Circular	Kammtail
Tube dimension [mm]	4.8	4.8	3 × 6
Horizontal tube rows	5	5	5
Vertical tube rows	9	9	9
Fin type	Wire	Wavy	Wavy
Fin spacing [mm]	5	10	10
Temperature outlet [K]	300.6	300.9	301
ΔP [Pa]	1.5	2.1	1.8
Fin area [m^2]	0.13	0.17	0.17
Tube area [m^2]	0.090	0.090	0.079
Total area [m^2]	0.22	0.26	0.25
ΔT_{lm} [K]	18.7	18.5	18.4
Q-total [W]	105.7	129.7	129.9
h-total [W/m^2K]	25.8	26.6	28.1
q-total [W/m^2]	480.5	493.1	518.0

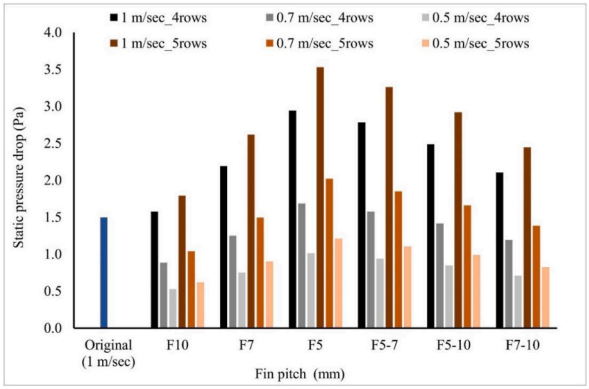


Fig. 15. Effect of variations in fin spacing, tube row number, and air velocity on pressure drop in inline arrangement.

Fig. 17 illustrates the change in the static pressure drop on the condenser between the staggered and inline tube arrangement solely for the homogenous fin arrangement. The findings indicate similar trends in both arrangements with an increase in static pressure drop versus increasing velocities. One of the most significant parameters influencing the condensers' air-side performance is the gap between the fins. As previously noted, in the staggered tube arrangement, reducing the fin pitch from 10 mm to 5 mm resulted in a pressure drop increase of 29.9–72% depending on air velocity. It was observed that the static pressure drop of the staggered arrangement increases by 8%–28.2% when compared to the inline arrangement for a velocity of 1 m/s.

Fig. 18 illustrates the change in the average heat-transfer coefficient on the condenser to allow an evaluation of the effect of fin spacing ranging from 5 mm to 10 mm for the staggered tube configuration under distinct air velocity levels. Upon examining Fig. 18, it becomes apparent that an increase in fin pitch leads to an increase in the heat-transfer coefficient. The convective heat-transfer

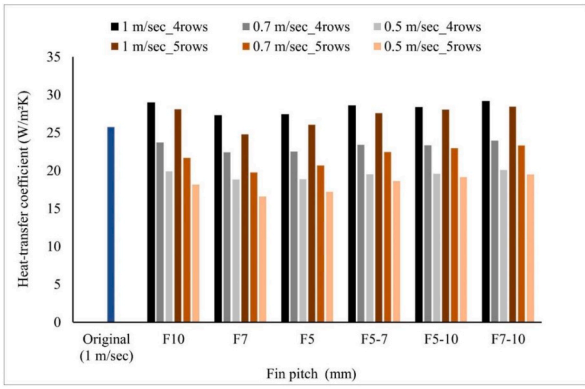


Fig. 16. The variation in total heat-transfer coefficient with respect to changes in fin spacing, tube row number, and air velocity for inline arrangement.

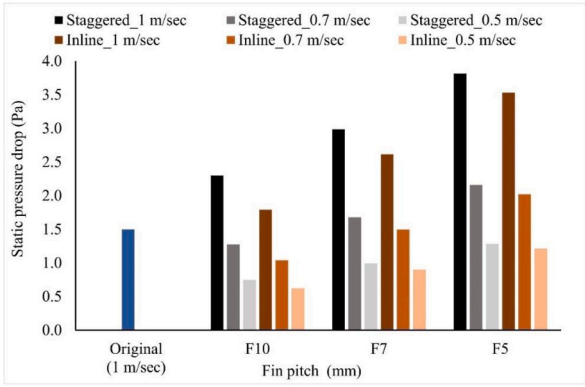


Fig. 17. Variation of static pressure drop with changing fin spacing and air velocity for both staggered and inline arrangements of 5 rows of tubes.

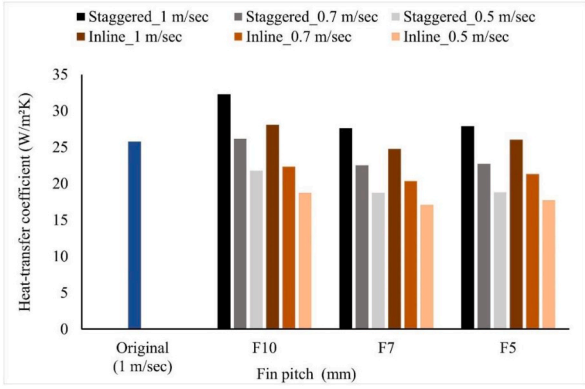


Fig. 18. Variation of total heat-transfer coefficient according to the variation of fin spacing and air velocity for staggered versus inline arrangement for 5 rows of tubes.

coefficient for the free-stream air velocity of 1 m/s is about 27.9 W/m^{2}K for a fin pitch of 5 mm and 32.3 W/m^{2}K for a fin pitch of 10 mm under identical flow conditions. The rise in heat-transfer coefficient is approximately 15.7%. Compared to an inline arrangement, the convection heat-transfer coefficient of a staggered arrangement increases by 6–17.1%, as demonstrated in Fig. 18. A staggered arrangement results in greater heat transfer at the same air velocity and produces higher pressure drops compared to an inline arrangement due to increased turbulence. This phenomenon is well established in the literature [30].

Fig. 19 shows the effect of inline and staggered tube arrangement on the velocity and pressure distribution. When staggered tube arrangement was applied with the same number of tubes, same fin spacing and air velocity, it was observed that the pressure loss increased by 12% and the heat transfer increased by 7.7% due to the increase in inter-tube turbulence and velocity. This result is expected and well known from the literature [23,30].

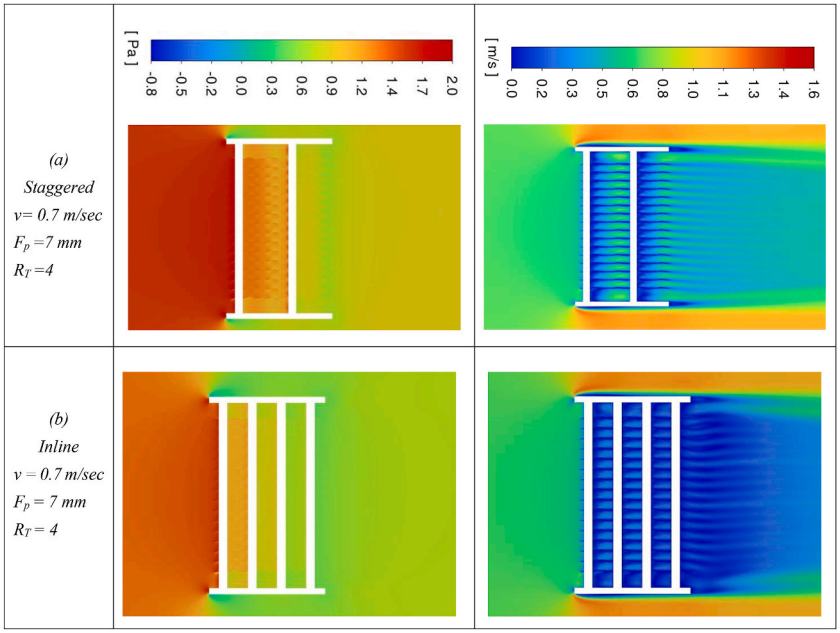


Fig. 19. Pressure and velocity distribution for staggered versus inline arrangement for 4 rows of tubes (a) staggered design, (b) inline design.

As per Table 1, after the analysis, two alternative designs were found to replace the original condenser. Option-1 is characterized by a 4-row staggered tube arrangement with a homogeneous wavy fin shape, spaced 7 mm apart. For this setup, the air speed is 0.7 m/s. Option-2, on the other hand, features a 4-row inline tube arrangement with a hybrid wavy fin structure, spaced between 7 and 10 mm apart for the free-stream air velocity of 0.7 m/s. Compared to the original condenser, the Option-1 design shows a 7% reduction in

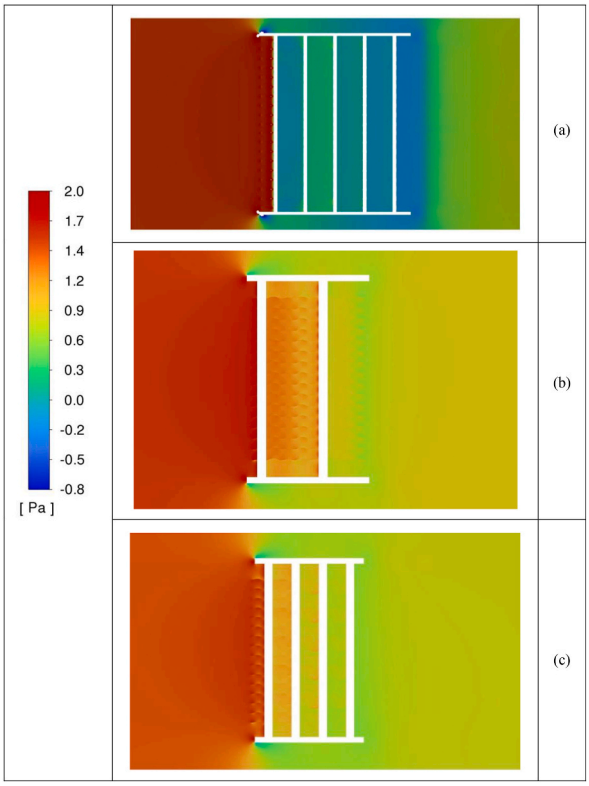


Fig. 20. Pressure contours: (a) original condenser, (b) alternative Option-1 design, (c) alternative Option-2 design (air flow is from left to right).

static pressure drop and a 5% decrease in heat-transfer coefficient. The overall heat transfer, however, increases by 12.2%. This improved performance is achieved at a lower air velocity of 0.7 m/s and with 4 rows of tubes, resulting in a 30% reduction in air flow rate demand and a design that is 20% more compact. With the Option-2 design, the pressure drop decreases by 20.4% while the overall heat-transfer coefficient decreases by 7%. However, the overall heat transfer improves by 5.6%. There is also a 17.7% increase in total surface area. Furthermore, this design shows a significant decrease in air flow rate by 30% and a corresponding 20% reduction in the volume of the condenser. These designs also lead to a decreased noise level and the use of a smaller fan.

Fig. 20, Figs. 21 and 22 display the pressure, velocity and temperature contours on the symmetry plane for the original, Option-1, and Option-2 designs shown in Table 11, respectively. As shown in Figs. 20 and 21, the wake region formed by the leading first wire of the original condenser results in a reduction in the velocity of the airflow reaching the following wire. The heat-transfer rate from the back wires is reduced due to the decrease in velocity and increase in temperature within the gap. Compared to the original condenser, the Option-1 design shows that there is a reduced weak region in the gap between tubes due to the staggered tube arrangement, resulting in increasing turbulence and the formation of a zone of higher velocity. This phenomenon leads to an increase in temperature and heat transfer behind the tube. When examining Option-2, it is observed that there is an increase in the heat transfer due to the temperature increase at the heat exchanger outlet, whereas along the tube and fin, a low-velocity region is formed due to the inline arrangement. It was observed that the pressure drop between the tubes for the original case is higher compared to the two alternative designs. This shows that the fin shape, fin and tube placement improved velocity distribution and pressure loss.

4. Conclusion

This study focused on an experimental and numerical analysis of the thermal characteristics of wavy fin-on-Kammtail tube condensers as an alternative to conventional wire-on-tube condensers. After validating the CFD model through experimental investigations, a numerical parametric study was conducted. The study aimed to investigate the impact of air velocity, fin pitches, row number of tubes, and tube and fin arrangement on the air-side performance of the condenser. The research and its findings may be summarized as follows.

- A novel design referred to as “Kammtail tube shape with wavy fins”, characterized by a streamlined structure that aims to delay flow separation with a primary objective of enhancing the aerodynamic efficiency of the original wire-on-tube condenser, was studied.
- This study aimed to analyze the influence of different turbulence models, namely the k-ε standard wall, RNG k-ε, k-ε realizable, and k-ω SST models. It was concluded that the k-ω SST model provided the most accurate results compared to the experimental values, with deviations of less than 10%.

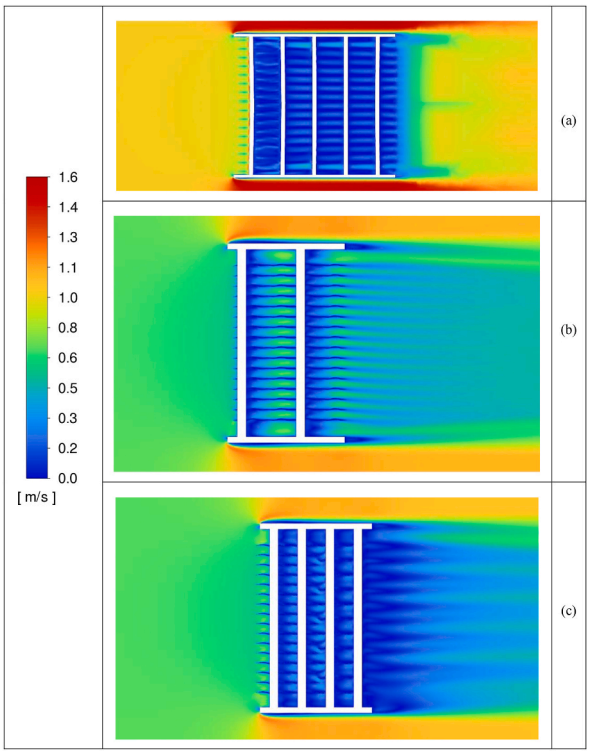


Fig. 21. Velocity contours: (a) original condenser, (b) alternative Option-1 design, (c) alternative Option-2 design (air flow is from left to right).

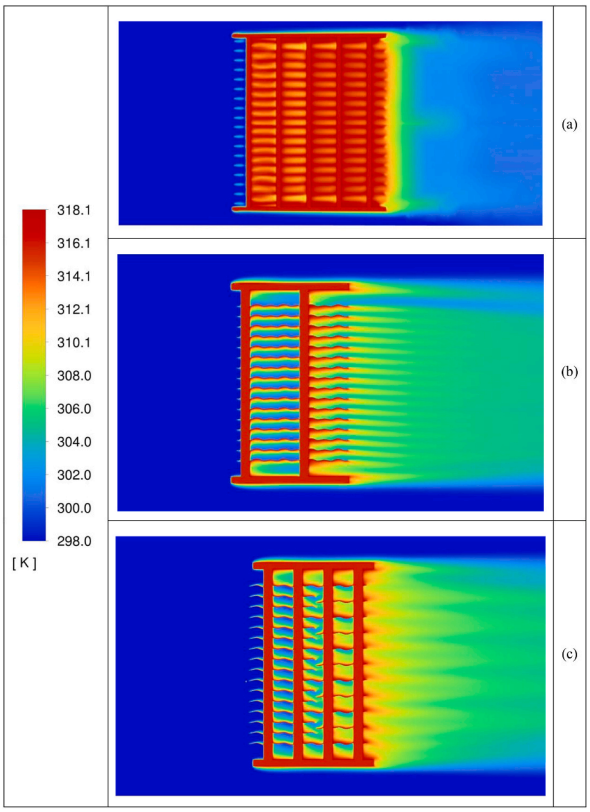


Fig. 22. Temperature contours: (a) original condenser, (b) alternative Option-1 design, (c) alternative Option-2 design (air flow is from left to right).

Table 11
Alternative designs to the original wire-on-tube condenser.

	Original	Option-1	Option-2
Tube profile	Circular	Kammtail	Kammtail
Tube dimension [mm]	4.8	3 × 6	3 × 6
Horizontal tube rows	5	4	4
Tube arrangement	Inline	Staggered	Inline
Fin type	Wire	Wavy	Wavy
Fin spacing [mm]	5	7	7–10
Fin arrangement	Homogeneous	Homogeneous	Hybrid
Air velocity [m/sec]	1	0.7	0.7
Fin area [m^2]	0.13	0.21	0.18
Tube area [m^2]	0.09	0.063	0.079
Total area [m^2]	0.22	0.27	0.26
Temperature outlet [K]	300.6	302.3	301.9
ΔP [Pa]	1.5	1.4	1.2
ΔT_{lm} [K]	18.7	17.8	18.0
Q-total [W]	105.7	118.6	111.6
h [W/m^2K]	25.8	24.5	24
q-total [W/m^2]	480.5	434.3	430.8

- The separation points where the x-wall shear stress is zero were determined for the circular, and k-form 3 × 6 mm as 0.59 and 0.78, respectively.
- The separation point shifted as expected with the alternative tube design. As a result, the pressure drop was reduced and the contact area between the fluid and the solid surface increased for the 3 × 6 mm kammtail form compared to the original circular tube.
- Based on CFD calculations, the condenser dissipated total heat of 105.7 W while experiencing a pressure drop of 1.5 Pa. The CFD analysis findings indicated a high level of concurrence with experimental results on heat transfer and pressure drop, with less than 10% deviation.
- It was discovered that, for the same fin types and fin surface areas, the Kammtail tube shape yielded 19% lower pressure drop and 9% higher heat-transfer coefficient compared to the original circular tube profile.

- As the air velocity increased from 0.5 m/s to 1 m/s, the static pressure drop increased by up to 66.6% and the heat-transfer coefficient increased in the range of 18–33.4%. When the fin pitch was reduced, the static pressure drop increased between 32.9% and 97%, and the heat-transfer coefficient decreased by roughly 4.7–11.7% depending on the air velocity.
- The reduction of the number of tube rows from 5 to 4 resulted in the total surface area and flow resistance decreasing in the direction of the flow. As a result, pressure drop decreased by 12.1–16.6% and the heat-transfer coefficient increased by up to 10%.
- It was observed that for a velocity of 1 m/s, the staggered arrangement resulted in an increase of 8–28.2% in static pressure drop and 6–17.1% in heat-transfer coefficient compared to the inline arrangement due to turbulence.
- Compared to the original condenser at 1 m/s air velocity and tube row number of 5, the pressure drop and the convection heat-transfer coefficient of the Kammtail tube condenser decreased between %5.1–40.9 and %7–13, respectively, depending on the fin spacing for tube row number of 4 and air velocity of 0.7 m/s. Furthermore, total heat transfer rate increased by 4.2%–23.8%.
- A detailed analysis led to the identification of two new alternative designs to replace the original condenser, which exhibited decreases of 7–20.4% in static pressure drop and increases of 5.6–12.2% in heat transfer compared to the original condenser.
- Enhanced performance was attained through reduced air velocity (0.7 m/s) and tube row number (4 rows). Additionally, the new designs displayed a sizeable decrease in airflow by 30% and a concurrent reduction in condenser volume by 20%.

CRediT authorship contribution statement

Funda Erdem Şahnali: Writing – original draft, Methodology, Investigation, Formal analysis, Data curation, Conceptualization. **Ş. Özgür Atayılmaz:** Writing – review & editing, Supervision. **Zafer Gemici:** Writing – review & editing, Supervision.

Declaration of competing interest

The authors declare that they have no known competing financial interests or personal relationships that could have appeared to influence the work reported in this paper.

Data availability

No data was used for the research described in the article.

Acknowledgments

The authors would like to thank Arçelik Central R&D for providing the test chambers, measurement instruments, and financial support for this study.

References

[1] IEA, Data and statistics, IEA (2023). https://www.iea.org/data-and-statistics/charts. (Accessed 11 October 2023).
[2] S. Wongwises, Y. Chokeman, Effect of fin pitch and number of tube rows on the air side performance of herringbone wavy fin and tube heat exchangers, Energy Convers. Manag. 46 (2005) 2216–2231, https://doi.org/10.1016/j.enconman.2004.09.011.
[3] A. Nuntaphan, T. Kiatsiriroat, C.C. Wang, Air side performance at low Reynolds number of cross-flow heat exchanger using crimped spiral fins, Int. Commun. Heat Mass Tran. 32 (2005) 151–165, https://doi.org/10.1016/j.icheatmasstransfer.2004.03.022.
[4] A. Erek, B. Özerdem, L. Bilir, Z. Ilken, Effect of geometrical parameters on heat transfer and pressure drop characteristics of plate fin and tube heat exchangers, Appl. Therm. Eng. 25 (2005) 2421–2431, https://doi.org/10.1016/j.applthermaleng.2004.12.019.
[5] A. Kumar, J.B. Joshi, A.K. Nayak, A comparison of thermal-hydraulic performance of various fin patterns using 3D CFD simulations, Int. J. Heat Mass Tran. 109 (2017) 336–356, https://doi.org/10.1016/j.ijheatmasstransfer.2017.01.102.
[6] X. Liu, J. Yu, G. Yan, A numerical study on the air-side heat transfer of perforated finned-tube heat exchangers with large fin pitches, Int. J. Heat Mass Tran. 100 (2016) 199–207, https://doi.org/10.1016/j.ijheatmasstransfer.2016.04.081.
[7] X. Li, D. Zhu, J. Sun, X. Mo, Y. Yin, Air side heat transfer and pressure drop of H type fin and tube bundles with in line layouts, Exp. Therm. Fluid Sci. 96 (2018) 146–153, https://doi.org/10.1016/j.expthermflusci.2018.02.029.
[8] R. Romero-Méndez, M. Sen, K.T. Yang, R. McClain, Effect of fin spacing on convection in a plate fin and tube heat exchanger, Int. J. Heat Mass Tran. 43 (2000) 39–51, https://doi.org/10.1016/S0017-9310(99)00120-9.
[9] P. Wais, Fin-tube heat exchanger performance for different louver angles, Scientific Letters of Rzeszow University of Technology - Mechanics 31 (2014) 115–122, https://doi.org/10.7862/rm.2014.13.
[10] A. Morales-Fuentes, Y.A. Loredo-Sáenz, Identifying the geometry parameters and fin type that lead to enhanced performance in tube-and-fin geometries, Appl. Therm. Eng. 131 (2018) 793–805, https://doi.org/10.1016/j.applthermaleng.2017.12.057.
[11] L. Zhao, X. Gu, L. Gao, Z. Yang, Numerical study on airside thermal-hydraulic performance of rectangular finned elliptical tube heat exchanger with large row number in turbulent flow regime, Int. J. Heat Mass Tran. 114 (2017) 1314–1330, https://doi.org/10.1016/j.ijheatmasstransfer.2017.06.049.
[12] M. Zeeshan, S. Nath, D. Bhanja, Numerical study to predict optimal configuration of fin and tube compact heat exchanger with various tube shapes and spatial arrangements, Energy Convers. Manag. 148 (2017) 737–752, https://doi.org/10.1016/j.enconman.2017.06.011.
[13] D.H. Park, D.B. Lee, E.R. Seo, Y.J. Park, Study on the heat transfer and fluid flow characteristics in V-shaped corrugated composite fin, Appl. Therm. Eng. 102 (2016) 293–301, https://doi.org/10.1016/j.applthermaleng.2016.03.047.
[14] A. Gholami, M.A. Wahid, H.A. Mohammed, Thermal–hydraulic performance of fin-and-oval tube compact heat exchangers with innovative design of corrugated fin patterns, Int. J. Heat Mass Tran. 106 (2017) 573–592, https://doi.org/10.1016/j.ijheatmasstransfer.2016.09.028.
[15] C.W. Lu, J.M. Huang, W.C. Nien, C.C. Wang, A numerical investigation of the geometric effects on the performance of plate finned-tube heat exchanger, Energy Convers. Manag. 52 (2011) 1638–1643, https://doi.org/10.1016/j.enconman.2010.10.026.
[16] P. Pongsoi, P. Promoppatum, S. Pikulkajorn, S. Wongwises, Effect of fin pitches on the air-side performance of L-footed spiral fin-and-tube heat exchangers, Int. J. Heat Mass Tran. 59 (2013) 75–82, https://doi.org/10.1016/j.ijheatmasstransfer.2012.11.071.
[17] Z.M. Lin, L.B. Wang, Y.H. Zhang, Numerical study on heat transfer enhancement of circular tube bank fin heat exchanger with interrupted annular groove fin, Appl. Therm. Eng. 73 (2014) 1465–1476, https://doi.org/10.1016/j.applthermaleng.2014.05.073.
[18] A. Gönül, Ö. Ağra, Ö. Atayılmaz, H. Demir, M.K. Sevindir, İ. Teke, Experimental and numerical investigation of air-side forced convection on wire-on-tube condensers, Int. J. Therm. Sci. 151 (2020), https://doi.org/10.1016/j.ijthermalsci.2019.106241.

[19] Y. Maghsoudali, A. Rastegarkoutenaei, M. Sahami, M.G. Bandpy, Experimental investigating the thermal and hydraulic performance of heat exchangers with helix wire finned tube, Appl. Therm. Eng. 231 (2023), https://doi.org/10.1016/j.applthermaleng.2023.120919.
[20] R.S. Espíndola, J. Boeng, F.T. Knabben, C.J.L. Hermes, A new heat transfer correlation for natural draft wire-on-tube condensers for a broad geometry span, Int. J. Refrig. 114 (2020) 10–18, https://doi.org/10.1016/j.ijrefrig.2020.02.025.
[21] I. Made Arsana, R. Agung Wahyuono, Design, performance, and optimization of the wire and tube heat exchanger, in: Heat Exchangers, IntechOpen, 2022, https://doi.org/10.5772/intechopen.100817.
[22] G. Peker, D. Burcu Özkan, Performance evaluation of hot-wall condenser in a domestic refrigerator, Appl. Therm. Eng. 233 (2023), https://doi.org/10.1016/j.applthermaleng.2023.121137.
[23] Z. Gemici, M. Budakli, Numerical study of the intensification of single-phase heat transfer in a sandwich-like channel using staggered miniature-pin fins, Numeri Heat Transf A Appl (2023) 1–34, https://doi.org/10.1080/10407782.2023.2202883.
[24] Ansys, Ansys Fluent Theory Guide, 2022.
[25] H. Pourdel, H.H. Afrouzi, O.A. Akbari, M. Miansari, D. Toghraie, A. Marzban, A. Koveiti, Numerical investigation of turbulent flow and heat transfer in flat tube: effect of dimples with operational goals, J. Therm. Anal. Calorim. 135 (2019) 3471–3483, https://doi.org/10.1007/s10973-018-7529-8.
[26] R. Hosseinnezhad, O.A. Akbari, H. Hassanzadeh Afrouzi, M. Biglarian, A. Koveiti, D. Toghraie, Numerical study of turbulent nanofluid heat transfer in a tubular heat exchanger with twin twisted-tape inserts, J. Therm. Anal. Calorim. 132 (2018) 741–759, https://doi.org/10.1007/s10973-017-6900-5.
[27] F.R. Menter, Two-equation eddy-viscosity turbulence models for engineering applications, AIAA J. 32 (1994) 1598–1605, https://doi.org/10.2514/3.12149.
[28] C.L. Rumsey, P.R. Spalart, Turbulence model behavior in low Reynolds number regions of aerodynamic flowfields, in: 38th AIAA Fluid Dynamics Conference and Exhibit, 2008. Seattle.
[29] C.K. Mangrulkar, A.S. Dhoble, S.G. Chakrabarty, U.S. Wankhede, Experimental and CFD prediction of heat transfer and friction factor characteristics in cross flow tube bank with integral splitter plate, Int. J. Heat Mass Tran. 104 (2017) 964–978, https://doi.org/10.1016/j.ijheatmasstransfer.2016.09.013.
[30] Y.A. Çengel, A.J. Ghajar, Heat and Mass Transfer : Fundamentals & Applications, sixth ed., McGraw-Hill Education, 2020.
[31] B. Valbracht, Laboratory methods of testing induced flow fans for rating, the development of AMCA standard 260-07, in: AMCA International Engineering Conference, Las Vegas, 2008.
[32] IEC 62552, IEC 62552:2015 Household Refrigerating Appliances –Characteristics and Test Methods, 2015.
[33] T.-H. Lee, J.-Y. Yun, J.-S. Lee, J.-J. Park, K.-S. Lee, Determination of airside heat transfer coefficient on wire-on-tube type heat exchanger, Int. J. Heat Mass Tran. 44 (2001) 1767–1776, https://doi.org/10.1016/S0017-9310(00)00201-5.
[34] S.J. Kline, F.A. McClintock, Describing uncertainties in single sample experiments, J. Inst. Eng. 75 (1953) 3–8.
[35] E.G. Chijioke, Modelling of the Laminar to Turbulent Flow Transition in a Compressor Cascade, Bachelor of Science, Warsaw University of Technology, 2012.